energies

MDPI

Article

A Grid-Supporting Photovoltaic System Implemented by a VSG with Energy Storage

Huadian Xu, Jianhui Su, Ning Liu * and Yong Shi

School of Electrical Engineering and Automation, Hefei University of Technology, Hefei 23009, China; xuhuadian@mail.hfut.edu.cn (H.X.); su_chen@hfut.edu.cn (J.S.); shiyong@hfut.edu.cn (Y.S.)

* Correspondence: Ning.Liu@unb.ca; Tel.: +86-551-6290-4042

Received: 24 October 2018; Accepted: 8 November 2018; Published: 14 November 2018

check for updates

Abstract: Conventional photovoltaic (PV) systems interfaced by grid-connected inverters fail to support the grid and participate in frequency regulation. Furthermore, reduced system inertia as a result of the integration of conventional PV systems may lead to an increased frequency deviation of the grid for contingencies. In this paper, a grid-supporting PV system, which can provide inertia and participate in frequency regulation through virtual synchronous generator (VSG) technology and an energy storage unit, is proposed. The function of supporting the grid is implemented in a practical PV system through using the presented control scheme and topology. Compared with the conventional PV system, the grid-supporting PV system, behaving as an inertial voltage source like synchronous generators, has the capability of participating in frequency regulation and providing inertia. Moreover, the proposed PV system can mitigate autonomously the power imbalance between generation and consumption, filter the PV power, and operate without the phase-locked loop after initial synchronization. Performance analysis is conducted and the stability constraint is theoretically formulated. The novel PV system is validated on a modified CIGRE benchmark under different cases, being compared with the conventional PV system. The verifications demonstrate the grid support functions of the proposed PV system.

Keywords: coordination control; energy storage; grid support function; inertia; photovoltaic; virtual synchronous generator

1. Introduction

This paper proposes a grid-supporting photovoltaic system, including implementation and performance analysis. In this section, the background, literature review, formulation of the problem of interest for this investigation, scope and contribution of this study, and organization of the paper are presented.

1.1. Background and Significance

Synchronous generators (SGs), which take responsibility for frequency regulation in electric power systems (EPS), operate as inertial voltage sources, providing the inertia to slow down frequency dynamics and moderate the power imbalance between generation and consumption in an autonomous fashion. Driven by issues such as potential exhaustion of conventional fossil fuel based energies (e.g., coal, oil, and natural gas) and increasing environmental concerns, the quantity of renewable energy sources (RES) integrated into EPS is escalating [1,2]. In consequence, SGs are gradually being replaced by inverters with high penetration of RES.

Among RES, solar energy via photovoltaic (PV) systems is one of the most promising, and has largely penetrated the global energy market [3,4]. A decrease of investment costs, technological development, and governmental support has led to the significant increase in PV systems that has been seen in recent years, and there is still significant need for growth [1,5].

However, grid-connected inverters are controlled as current sources with phase-locked loops (PLL) in conventional PV systems [6], which turns conventional PV systems into power injectors and grid-following units [7,8]. As power injectors, conventional PV systems inject the power extracted from the PV array to EPS without the capability to mitigate the power imbalance between generation and consumption. Meanwhile, conventional PV systems, as grid-following units, provide little of the inertia that plays an essential role in short-term system stability [9], thus the increasing penetration of PV generators reduces the inertia of EPS, which exacerbates the system's stability [9–11]. Therefore, implementing the function of a supporting grid in PV systems, which offers inertia and participates in frequency regulation, is significantly beneficial to the stability enhancement of EPS.

1.2. Formulation of the Problem of Interest for This Study

Existing research mainly concentrates on the realization of a virtual synchronous generator (VSG) and the improvement of the performance of inverters that are assumed to be supplied by stiff DC voltage sources. However, rare attention has been paid to the realization of a VSG in practical PV systems. It is a challenge to introduce inertia, the indispensable property for VSGs, into an inverter only powered by a PV system. To enable the inverter to emulate the inertia of SGs, an energy buffer, whose function is identical to a rotor for kinetic energy, needs to be installed at the dc link of the inverter.

The main objective of this paper is therefore to equip PV systems with the function of supporting the grid through emulating SG characteristics, then analyze the performance, formulate the stability constraint, and corroborate the implemented function with numerical experiments.

1.3. Literature Review

Virtual synchronous generator (VSG) technology, which controls inverters to mimic the characteristics of SGs to provide inertia and participate in the frequency regulation of EPS, emerged in response to issues addressed in Section 1.2 [12–15]. The core of VSG technology is to present the various energy sources interfaced to the grid through power electronic converters as SGs [16]. Researches on VSGs in References [12–15] are devoted to realizing the basic function of emulating inertia using converters. Recently, VSG research focus towards developing novel control strategies, and improving the performance of these strategies from the point-of-view of enhanced dynamics, stability, and so on. Compared with the method investigated in Reference [14], the filter inductance of the synchronverter studied in Reference [17] is virtually increased to improve the stability. In the early Ise lab's topology presented in Reference [15], active power oscillation becomes one of the major concerns during the emulation of inertia [18]. In Reference [18], an alternating moment of inertia is proposed to suppress such oscillation. Furthermore, the self-adaptive inertia and damping approach is presented to improve the dynamics in Reference [19]. To smooth transitions and reduce frequency excursions, a particle swarm optimization technique was developed in Reference [20], a self-tuning VSG was investigated in Reference [21] and an auxiliary loop is proposed to adjust the dynamic response speed through correct the damping in Reference [22].

In References [14,23], inverters that mimic SGs were studied with an assumption that inverters are supplied by stiff DC voltage sources, but inverters only energized by PV systems cannot satisfy this assumption. In Reference [24], a VSG was realized by a battery/ultracapacitor hybrid ES system, but the inverters based on RES were not competent in emulating the characteristics of SGs. In References [15,25], it is pointed out that energy storage (ES) should be installed to emulate the kinetic energy stored in the rotating rotors of SGs, but the detailed system topology is not considered, nor is the control strategy coordinating ES and the renewable energy generator. In References [26,27], ES is applied to a PV system to smooth power fluctuation, and this system possesses no characteristics of SGs. In Reference [28], a battery is used as the backup for a PV inverter that employs only PQ control or droop control, causing the inverter to operate unlike SGs.

1.4. Scope and Contribution of This Study

Motivated by the above observations, this paper presents a novel grid-supporting PV system, achieving emulation of SG characteristics. Consequently, the grid-supporting PV system, behaving as SGs, contributes to supporting the grid by autonomously mitigating the power imbalance between generation and consumption, and slowing down frequency dynamics with virtual inertia. Accordingly, the proposed grid-supporting PV system is superior to the conventional PV system, while the conventional PV system cannot moderate the deficits and surplus of power in the grid, and is unable to provide inertia.

1.5. Organization of the Paper

The content of this paper is organized as follows: Section 2 introduces the topology and control scheme. In Section 3, performance analysis is conducted, and the stability constraint is obtained through the established small-signal model. Results of case studies conducted on a modified CIGRE LV network benchmark are presented and discussed in Section 4. Section 5 draws the conclusions of this paper and discusses future research directions.

2. Topology and Control Scheme

Figure 1 shows the topology and control scheme of the grid-supporting PV system. In order to mimic the kinetic energy stored in the rotating rotors of SGs, an energy storage (ES) unit equipped with a bidirectional DC-DC converter was installed in the conventional PV system. Accordingly, the hardware consists of an ES unit, a bidirectional DC-DC converter, an inverter, and a PV array. The PV array was tied directly to the dc link, sharing the same dc bus with the DC-DC converter and the inverter. A buck/boost converter is adopted in this paper.

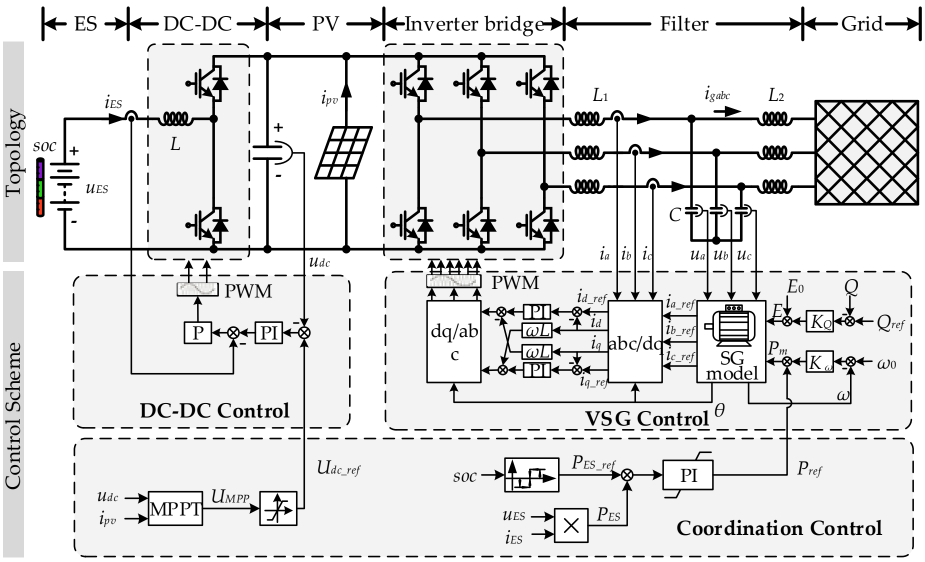

Figure 1. Topology and control scheme of the grid-supporting PV system.

As Figure 1 depicts, the overall control scheme of the grid-supporting PV system comprises three strategies: DC-DC control, VSG control, and coordination control. The coordination control is designed to attune the system with two tasks: (1) One is to ascertain the value of the dc link voltage reference U_{dc_ref}, utilizing a maximum power point tracking (MPPT) algorithm to draw maximum power from the PV array. U_{dc_ref} is provided for DC-DC control, which performs the regulation of dc link voltage u_{dc}. (2) Another is to constrain the state of charge (SOC) of the ES unit through regulating the inverter active power reference P_{ref}, which capacitates the buck/boost to control u_{dc} for the inverter emulating SGs. P_{ref} is delivered to the VSG control that drives the inverter to emulate the characteristics of SGs.

The conventional PV system is only energized by PV input, and its interface inverter is controlled by a voltage-oriented control method, with an outer dc link voltage control loop and an inner current control loop [29]. As shown in Figure 1, the proposed grid-supporting PV system however, is energized by a PV array and ES unit, and the interface inverter is driven by the VSG control. Benefiting from the topology and control scheme, which are different from those of the conventional PV system, the grid-supporting PV system is able to provide inertia and participate in frequency regulation as SGs.

2.1. Coordination Control

To behave as an energy buffer like a rotating rotor, the ES unit must have not only energy to release, but also capacity to store absorbed energy. Therefore, the SOC of the ES unit must be kept within a proper range. Meanwhile, it is necessary to constrain the SOC to control the dc link voltage u_{dc}, so that the ES unit can release energy when u_{dc} falls, and store the absorbed energy when u_{dc} rises.

To constrain the SOC, the exchanged power P_{ES} (positive for discharge and negative for charge) between the ES unit and the dc link must be regulated. However, P_{ES} cannot be directly controlled by the buck/boost converter, which is resulted from that the DC-DC control performs the regulation of u_{dc}.

According to the law of conservation of energy, the following equation is obtained when the energy change of the capacitor at the dc link is ignored:

$$P_{ES} + P_{pv} = P_e \tag{1}$$

where P_{pv} is the power generated by the PV array, and P_e is the output active power of the inverter in the system.

Since the PV array operates at the maximum power point, P_{pv} in Equation (1) fails to adjust. Thus, regulating P_e is the only way to control P_{ES}. Due to the emulated SG characteristics of the inverter, P_e can be controlled with coordination control through regulating the inverter active power reference P_{ref}. To track the exchanged power reference P_{ES_ref}, a proportional-integral (PI) regulator, whose input is the error between P_{ES_ref} and P_{ES}, is used for generating P_{ref}. Then, P_{ref} can be expressed as

$$P_{ref} = G_{PI}(s)\left(P_{ES\_ref} - P_{ES}\right) \tag{2}$$

where $G_{PI}(s) = K_p + K_i/s$ is the transfer function of the PI regulator, K_p and K_i are the proportional coefficient and integral coefficient of the PI regulator, respectively, and s is the Laplace operator.

The relationship of exchanged power reference P_{ES_ref} with respect to the SOC is designed as shown in Figure 2, where SOC_M is the mean of lower limit SOC_L and higher limit SOC_H, and P_0 is the absolute value of the charge power and the discharge power. The ES unit starts charging once the SOC is less than SOC_L, and discharging when the SOC is more than SOC_H. Both charging and discharging are terminated when the SOC reaches SOC_M. Applying the curve shown in Figure 2 to specify P_{ES_ref}, frequent operations of charge/discharge near SOC_L/SOC_H can be avoided by the coordination control. As the charge power and the discharge power of the ES unit depend on P_0, the rated power of the inverter and the charge-discharge rate (C-rate) of the ES unit need to be taken into account when determining P_0. First, the charge power and the discharge power of the ES unit should not be more than the rated power of the inverter to protect the inverter from over-current. Second, P_0 should ensure the charge current and the discharge current do not exceed the maximum C-rate so that the cycling life and the capacity of the ES unit are not significantly affected.

The dc link voltage reference U_{dc_ref} is generally equal to U_{MPP}, which is calculated by a maximum power point tracking (MPPT) algorithm, to ensure that the PV array operates at the point where it can output maximum power. Incremental Conductance [30,31], a classical MPPT algorithm, is employed in this paper.

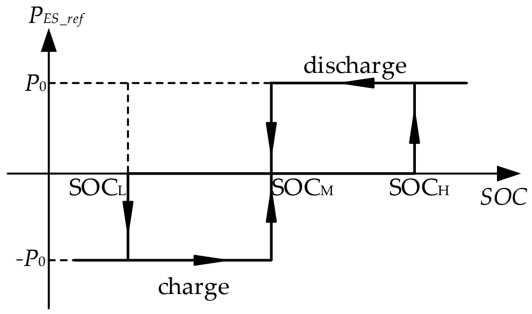

Figure 2. Relationship between exchanged power reference and SOC.

2.2. VSG Control

The VSG control aims to equip the inverter with the characteristics of a SG so that the inverter is capable of behaving like the SG. To realize the inverter emulating the characteristics of the SG, there are three sub-processes to implement during one carrier cycle, as illustrated in Figure 1. The voltages of the filter capacitors, u_a, u_b and u_c, are measured in real time, and virtualize the phase terminal voltages of the stator windings and serve as the input variables of a SG model. Through solving the model, the stator currents of the SG, i_{a_ref}, i_{b_ref}, and i_{c_ref}, are obtained as the reference currents for the inverter. To complete the emulation of the SG characteristics, the inverter output currents should be driven to track the reference currents. Thus, proportional-integral (PI) regulators in the rotating frame are employed to control the inverter.

The SG model adopted in this work comprises third-order electrical equations and second-order mechanical equations. The electrical equation set, which reproduces the stator circuit of the SG, is given by

$$L_s \frac{\mathrm{d}\boldsymbol{i_{abc\_ref}}}{\mathrm{d}t} = \boldsymbol{e_{abc}} - \boldsymbol{u_{abc}} - R_s \boldsymbol{i_{abc\_ref}} \tag{3}$$

where $\boldsymbol{u_{abc}} = [u_a,\ u_b,\ u_c]^{\mathrm{T}}$ denotes the phase terminal voltages of the stator windings; R_s and L_s are respectively the stator resistance and the stator inductance; $\boldsymbol{i_{abc\_ref}} = [i_{a\_ref},\ i_{b\_ref},\ i_{c\_ref}]^{\mathrm{T}}$ represents the currents of the stator windings, which serve as reference currents for the inverter; and $\boldsymbol{e_{abc}} = [e_a, e_b, e_c]^{\mathrm{T}} = E[\sin\theta, \sin(\theta - 2\pi/3), \sin(\theta + 2\pi/3)]^{\mathrm{T}}$ denotes the induced phase electromotive forces in the stator windings.

The electromechanical characteristics of the SG, neglecting the mechanical losses and considering the effect of damper windings, can be described as

$$2H \frac{\mathrm{d}\omega}{\mathrm{d}t} = \frac{P_m}{\omega} - \frac{P_e}{\omega} - D(\omega - \omega_0) \tag{4}$$

$$\frac{\mathrm{d}\theta}{\mathrm{d}t} = \omega \tag{5}$$

where H is the inertia constant, P_m is the mechanical power, D is the damping coefficient, ω and ω_0 are the actual and the nominal angular frequency, respectively, and θ is the electrical rotation angle.

To emulate the droop characteristics of the primary frequency control (PFC) and primary voltage control (PVC), P_m and E can be expressed as

$$P_m = P_{ref} + K_\omega(\omega_0 - \omega) \tag{6}$$

$$E = E_0 + K_Q(Q_{ref} - Q) \tag{7}$$

where K_ω is the unit power regulation, E_0 is the no-load electromotive force (EMF), Q_{ref} and Q are the reference value and the actual value of the inverter output reactive power, respectively, and K_Q is the voltage droop coefficient.

2.3. DC-DC Control

The objective of the DC-DC control is to keep the actual value of the dc link voltage u_{dc} equal to the voltage reference U_{dc_ref} provided by the MPPT algorithm of the coordination control. Regulating u_{dc} to track u_{dc_ref} enables the PV array to operate at the maximum power point. The DC-DC control strategy incorporates an outer voltage loop with an inner current loop, as depicted in Figure 1. Through DC-DC control, a stiff dc link voltage, which is required to emulate the inertia, is provided for the inverter.

The buck/boost converter works in BUCK mode and charges the ES unit to prevent u_{dc} from rising when $P_{pv} > P_e$. Under the condition of $P_{pv} < P_e$, the buck/boost converter operates in BOOST mode and discharges the ES unit to stop u_{dc} from dropping. This indicates that the ES unit behaves as an energy buffer, emulating a rotating rotor through complementing the deficit, or absorbing the surplus, of PV production.

3. Performance Analysis and Stability Constraint Formulation

In this section, a small signal per unit (pu) model that considers the Q-E droop control is established. Utilizing the model, performance analysis is conducted, the impact of the Q-E droop control on stability is investigated, and the stability constraint is obtained.

3.1. Small-Signal Modelling

Figure 3 depicts the equivalent circuit of the inverter when connected to the grid. In this figure, δ is the power angle; U_g is the amplitude of the grid voltage; $R_s + jX_s$ is the virtual stator impedance implemented by the VSG control; $R_g + jX_g$ is the grid impedance, which includes the line impedance; and the grid-side filter impedance $j\omega L_2$ and $P_e + jQ$ is the apparent power measured for the control scheme.

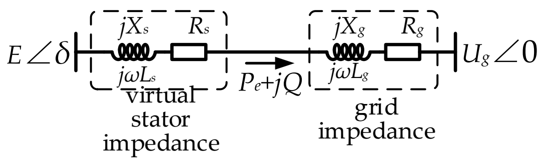

Figure 3. Equivalent circuit of the inverter when connected to the grid.

When R_s and R_g are neglected due to $X_s \gg R_s$ and $X_g \gg R_g$, P_e and Q can be expressed according to Figure 3 as follows:

$$P_e = \frac{EU_g}{X_s + X_g} \sin\delta \tag{8}$$

$$Q = \frac{1}{(X_s + X_g)^2}\left[X_g E^2 - X_s U_g^2 + (X_s - X_g) E U_g \cos\delta\right] \tag{9}$$

Linearizing P_e and Q with respect to E and δ, the deviations of P_e and Q are given by

$$\Delta P_e = k_{P\delta}\Delta\delta + k_{PE}\Delta E \tag{10}$$

$$\Delta Q = k_{Q\delta}\Delta\delta + k_{QE}\Delta E \tag{11}$$

where Δx ($x = P_e$, Q, E, and δ) represents the deviation of x, and

$$k_{P\delta} = \frac{\partial P_e}{\partial\delta} = \frac{EU_g}{X_s + X_g}\cos\delta \tag{12}$$

$$k_{PE} = \frac{\partial P_e}{\partial E} = \frac{U_g}{X_s + X_g}\sin\delta \tag{13}$$

$$k_{Q\delta} = \frac{\partial Q}{\partial \delta} = \frac{(X_g - X_s)EU_g}{(X_s + X_g)^2} \sin \delta \tag{14}$$

$$k_{QE} = \frac{\partial Q}{\partial E} = \frac{1}{(X_s + X_g)^2} \left[2X_g E + (X_s - X_g)U_g \cos \delta \right] \tag{15}$$

The small signal model of the *Q*-*E* droop control described by Equation (7) is given by

$$\Delta E = -K_Q \Delta Q \tag{16}$$

Solving Equations (10), (11), and (16), ΔP_e and ΔQ can be further derived as

$$\Delta P_e = (k_{p\delta} + \Delta K_S)\Delta\delta = K_S \Delta\delta \tag{17}$$

$$\Delta E = -\frac{K_Q k_{Q\delta}}{1 + K_Q k_{QE}} \Delta\delta = K_{\delta E} \Delta\delta \tag{18}$$

$$\Delta K_S = -\frac{K_Q k_{PE} k_{Q\delta}}{1 + K_Q k_{QE}} \tag{19}$$

Normalizing and linearizing Equations (4) and (5) yields [32]

$$\frac{\mathrm{d}\Delta\omega}{\mathrm{d}t} = \frac{1}{2H} [\Delta P_m - \Delta P_e - D\Delta\omega] \tag{20}$$

$$\frac{\mathrm{d}\Delta\delta}{\mathrm{d}t} = \frac{\mathrm{d}\Delta\theta}{\mathrm{d}t} - \omega_0 = \omega_0 \Delta\omega \tag{21}$$

where $\Delta\omega$ is the angular frequency deviation, ΔP_m is the deviation of P_m, D is the damping coefficient, H is the inertia constant in seconds, and ω_0 is the nominal angular frequency in rad/s.

The incremental Equations of (1), (2) and (6) are

$$\Delta P_{pv} + \Delta P_{ES} = \Delta P_e \tag{22}$$

$$\Delta P_{ref} = G_{PI}(s)\left(\Delta P_{ES\_ref} - \Delta P_{ES}\right) \tag{23}$$

$$\Delta P_m = \Delta P_{ref} - K_\omega \Delta\omega \tag{24}$$

By combining Equations (17)–(24), the small-signal model considering the *Q*-*E* droop control is established in Figure 4, and $\Delta\omega$ is correspondingly derived as Equation (25).

$$\Delta\omega = G(s)\left(\Delta P_{ES\_ref} + \Delta P_{pv}\right) \tag{25}$$

where the transfer function *G*(*s*) is given by

$$G(s) = \frac{(K_p s + K_i)s}{2Hs^3 + (D + K_\omega)s^2 + \omega_0 K_S (K_p + 1)s + \omega_0 K_S K_i} \tag{26}$$

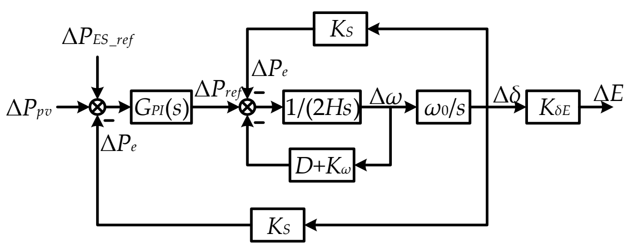

Figure 4. Small signal model of the grid-supporting PV system.

The expected performance of the grid-supporting PV system can be achieved if H, $D + K_\omega$, K_p, and K_i are properly selected in such a way that the poles of Equation (26) are located at desired locations.

3.2. Performance Analysis

The root loci family of the proposed PV system is shown in Figure 5a, where $2H$ = 1 s, 3 s, and 15 s, and $D + K_\omega$ changes from 10 pu to 200 pu. It is clear that H plays an important role in determining the settling time of the proposed PV system. As $D + K_\omega$ increases, the damping of the system rises and the stability is improved.

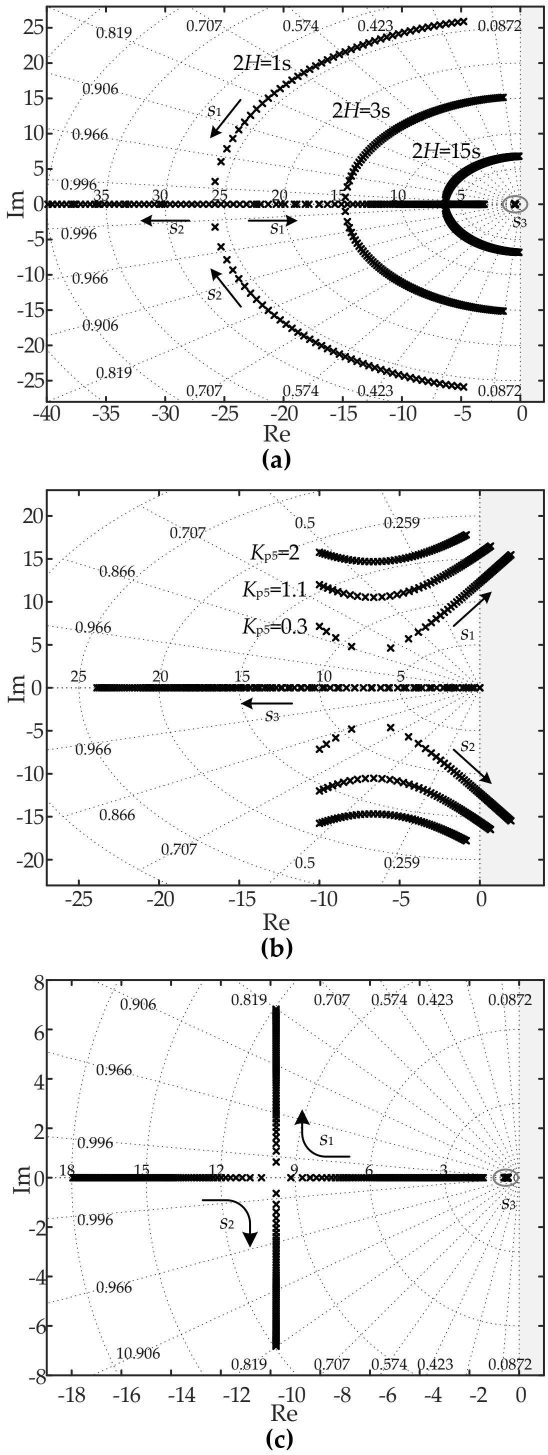

Figure 5. Family of root loci for variations of: (**a**) H and $D + K_\omega$; (**b**) K_p and K_i; (**c**) K_S.

Figure 5b depicts the root loci family considering variations of K_i from 0.1 pu to 50 pu, and K_p = 0.3 pu, 1.1 pu, and 2 pu. As Figure 5b shows, the damping drops, the overshoot rises, and the undamped natural frequency increases when K_p becomes larger. The damped frequency and the stability margin mainly depend on K_i. Instability may happen with an excessively large value of K_i. To ensure the stability of the system, it is necessary to formulate the constraint explicitly on H, $D + K_\omega$, K_p, and K_i to guide the tuning of parameters.

Figure 5c depicts the root locus where K_S varies from 0.5 pu to 2 pu. Among the three poles depicted in the plane, s_3 is the real root and its position depends on K_p and K_i. As K_S increases, the conjugate complex roots s_1 and s_2 evolve in the direction of the arrows. A larger K_S increases the real parts of s_1 and s_2, which improves the stability.

3.3. Impact of Q-E Droop Control on Stability

As Figure 5c illustrates, K_S is a factor that affects the stability of the grid-supporting PV system. According to Equation (17), K_s consists of two parts, $k_{P\delta}$ and ΔK_S. It is indicated in Equation (19) that ΔK_S is related to the coefficient K_Q of the *Q-E* droop control and embodies the impact of the *Q-E* droop control on the stability. When the *Q-E* droop control is invalidated (i.e., K_Q = 0) and only P-ω is considered, ΔK_S vanishes identically, and K_S in Equation (17) is equal to $k_{P\delta}$.

By substituting Equations (13)–(15) into Equation (19), ΔK_S can be obtained as Equation (27), where $r = X_g/X_S$. On the condition that the *Q-E* droop control works, K_Q is set to be a positive number. The power angle δ lies in the range from 0° to 90°, and E is generally larger than U_g. Thus, $k_{P\delta}$, k_{PE}, and k_{QE} are all positive. Accordingly, the curve of ΔK_S with respect to the ratio X_g/X_S is shown in Figure 6.

$$\Delta K_S \overset{r=X_g/X_S}{=} K_Q \cdot \frac{1-r}{1+r} \cdot \frac{EU_g^2 \sin^2\delta}{X_S^2(1+r)^2 + K_Q X_S\left[r(2E - U_g\cos\delta) + U_g\cos\delta\right]} \tag{27}$$

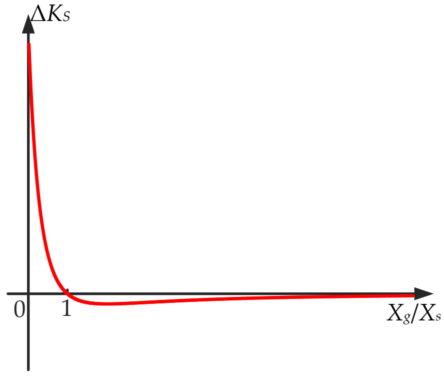

Figure 6. Curve of ΔK_S with respect to the ratio X_g/X_S.

As Figure 6 illustrates, ΔK_S is positive if the ratio X_g/X_S is less than 1, while ΔK_S is negative if the ratio X_g/X_S is greater than 1. Accordingly, K_S is greater than $k_{P\delta}$ under the condition of $X_g < X_S$, which means the *Q-E* droop control improves the stability, since a larger K_S improves the stability. Conversely, K_S is less than $k_{P\delta}$ when $X_g > X_S$, which indicates that the *Q-E* droop control worsens the stability in the weak grid. Besides, K_S is zero in the case of $X_g = X_S$, implying that the *Q-E* droop control has no effect on the stability.

3.4. Stability Constraint Formulation

The closed-loop system of Equation (26) is a third-order linear time-invariant. To analyze the stability, the Routh–Hurwitz stability criterion is used. The system characteristic equation is obtained from Equation (26) as

$$D(s) = a_0s^3 + a_1s^2 + a_2s + a_3 = 0 \tag{28}$$

where $a_0 = 2H$, $a_1 = D + K_\omega$, $a_2 = \omega_0 K_S (K_p + 1)$, and $a_3 = \omega_0 K_S K_i$.

Through applying the Routh–Hurwitz stability criterion to Equation (28), the system stability discriminant is yielded as

$$\begin{cases} a_i > 0, i = 0, 1, \ldots, 3 \\ a_1 a_2 - a_0 a_3 > 0 \end{cases} \tag{29}$$

Since H, $D + K_\omega$, K_p, and K_i are positive real numbers, the discriminant can be simplified as

$$\begin{cases} K_S > 0 \\ a_1 a_2 - a_0 a_3 > 0 \end{cases} \tag{30}$$

Substituting a_i into Equation (30) gives

$$\begin{cases} K_S > 0 \\ \frac{D+K_\omega}{2H} > \frac{K_i}{K_p+1} \end{cases} \tag{31}$$

Equation (31) presents the stability constraint for the grid-supporting PV system, which H, $D + K_\omega$, K_p, K_i, and K_S must satisfy to guarantee the stability of the system.

4. Results and Discussion

The proposed grid-supporting PV system was verified on the CIGRE benchmark of the European LV distribution network elaborated in Reference [33]. The topology of the benchmark is shown in Figure 7, and the line parameters of the benchmark are given in Table 1. All loads were configured to be balanced for simplicity. The apparent power and power factor (PF) of the loads are described in Figure 7. The 20 kV medium voltage grid in this benchmark was equated with a SG system with inertia constant of H = 9 s [32]. The PFC of the SG system reacts in 5 s when there is a frequency deviation, and the speed regulation of the PFC is 3.33%. Six cases were considered when disturbances occur, as listed in Table 2.

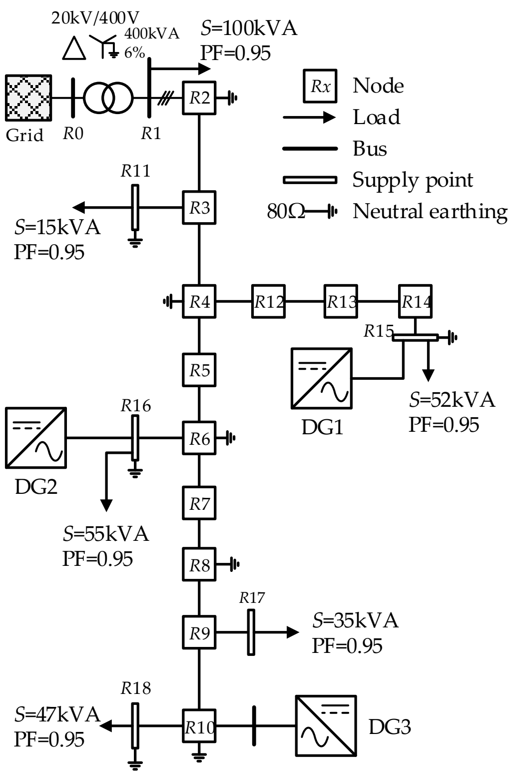

Figure 7. Modified benchmark of the European LV distribution network.

Table 1. Line parameters of the benchmark.

Node (From–To)	Length (m)	Resistance (mΩ)	Inductance (μH)
R1–R2	35	10.045	18.6052
R2–R3	35	10.045	18.6052
R3–R4	35	10.045	18.6052
R4–R6	70	20.09	37.2104
R6–R9	105	31.135	55.8156
R9–R10	35	10.045	18.6052
R4–R15	135	155.52	196.811
R6–R16	30	34.56	43.7358
R9–R17	30	34.56	43.7358
R10–R18	30	34.56	43.7358
Transformer	-	3.2	40.7437

Table 2. Cases Description.

Case	Disturbance	DG1–DG3
A	Sudden Load Variation	Conventional PV System
B		Proposed PV System
C	Short Circuit Fault	Conventional PV System
D		Proposed PV System
E	Step of Solar Irradiance	Conventional PV System
F		Proposed PV System

Case A and Case B considered sudden load variation by switching a load of 25 kW in R11 at 2 s. Case C and Case D considered a three-phase short circuit fault occurring at 2 s, the fault in each case was located at R17 and was cleared at 3 s. A step of solar irradiance from 1000 W/m^2 to 1050 W/m^2 was exerted on the PV array of DG3 at 2 s in Case E and Case F. After the disturbance occurred at 2 s in each case, the PFC was activated in 5 s; that is, at 7 s.

In Case A, Case C, and Case E, three conventional single-stage PV systems were applied to the benchmark as DG1−DG3. In comparison with the conventional PV system, three proposed grid-supporting PV systems, with parameters listed in Table 3, were connected to the feeder as DG1−DG3 in Case B, Case D, and Case F, and each ES unit was comprised of 25 Powersonic PS-121100 batteries in series. The SOC of each ES unit was set to 50%, which leads to $P_{ES\_ref} = 0$.

Table 3. Inverter Parameters of the Proposed PV System.

Meaning, Symbol, and Unit		No.1	No.2	No.3
Rated Power S_n (kVA)		20	20	50
Nominal frequency f_n (Hz)			50	
Nominal voltage V_n (V)			380	
Carrier frequency f_c (kHz)			10	
Filter values	L_1 (mH)	1.2	1.2	0.72
	C (μF)	20	20	50
	L_2 (mH)	0.8	0.8	0.18
Current loop controller gains	K_{cp} (pu)		2	
	K_{ci} (pu)		1500	
K_p (pu)			0.05	
K_i (pu)			0.3	
Parameter values of SG model	$2H$ (s)	10	14	10
	D (pu)	30	40	40
	R_s (pu)		0.08	
	L_s (pu)		0.8	
No-load EMF	E_0 (pu)		1.22	
Droop gains	K_ω (pu)	20	10	30
	K_Q (pu)		0	

To verify the functions of smoothing the power and tracking the maximum power point of the conventional PV system and the proposed grid-supporting PV system, solar irradiance steps were used in Case E and Case F to provide the most severe condition, although there is little possibility that the solar irradiance step would occur in a real case.

4.1. Case A: Sudden Load Variation—Conventional PV System

Figure 8a gives the resultant frequency of the grid, DG1, DG2, and DG3, respectively. All frequencies decrease consistently between 2 s and 5 s. With the phase-lock loop, the conventional PV system tracks the grid frequency (i.e., the LV distribution network frequency), but fails to provide the inertia due to operating as a grid-following unit. As depicted in Figure 8b, the output power of the conventional PV system injects power into the LV distribution network without change after the load variation, and thus is incapable of mitigating the power imbalance between generation and consumption. Figure 8c illustrates the dc link voltages, which are always regulated by the inverter of the conventional PV systems to perform MPPT.

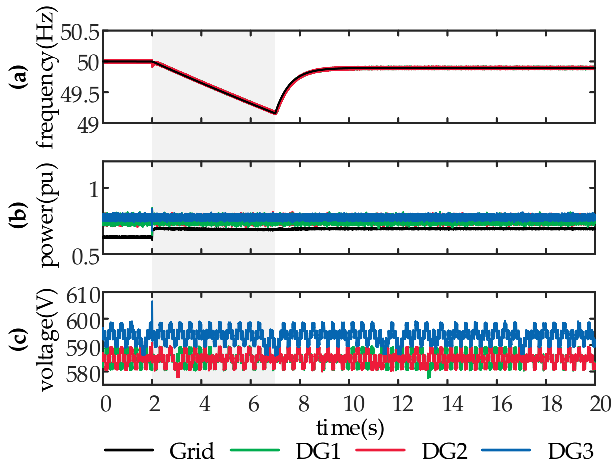

Figure 8. Responses to sudden load variation when conventional PV systems are applied as DG1–DG3: (**a**) Frequency response; (**b**) output active power; (**c**) dc link voltage of the inverter.

4.2. Case B: Sudden Load Variation—Proposed PV System

Figure 9 presents the responses when three proposed PV systems are integrated into the LV distribution network as DG1−DG3. As depicted in Figure 9a, all frequencies decrease between 2 s and 5 s, with a smaller rate of change of frequency (ROCOF) and higher frequency nadir when compared with Figure 8a of Case A. Through emulating the inertia of SGs, the proposed PV system is able to slow down frequency response and allow decent time for frequency control. Figure 9b shows that the proposed PV system mitigates the power imbalance between generation and consumption by increasing the output active power P_e autonomously, and thus supports the grid, mimicking the SG. Figure 9c plots the dc link voltage of the interface inverter, which is maintained at U_{MPP} by the buck/boost converter with the ES unit, even if there is an imbalance between P_{pv} and P_e. It is demonstrated that a stiff dc link voltage can be provided in the proposed PV system for the inverter to emulate the inertia. Figure 9d illustrates the exchanged power P_{ES} between the ES unit and the dc link. After the sudden load variation, the incremental of P_{ES} is consistent with that of P_e shown in Figure 9b. It is indicated that the ES unit balances the power between the PV array and the inverter, which emulates the behavior of a rotating rotor releasing kinetic energy when it's frequency drops. After PFC activation, the exchanged power P_{ES}, regulated by coordination control, gradually converges to P_{ES_ref} to constrain the SOC.

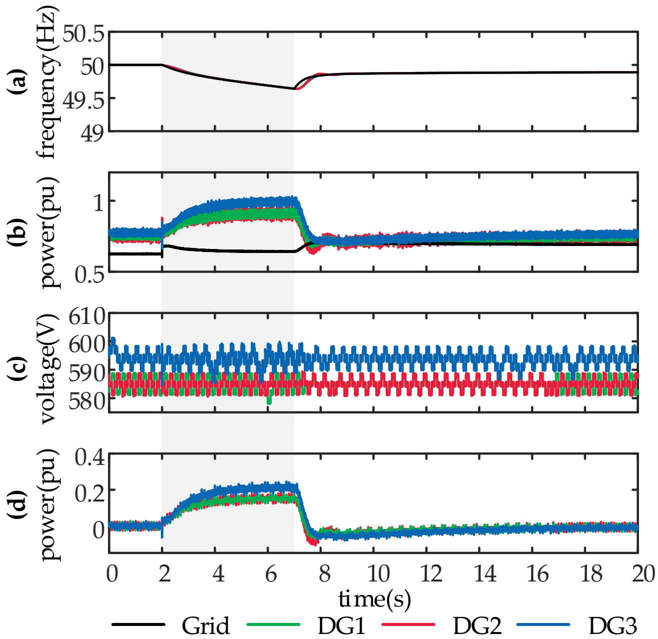

Figure 9. Responses to sudden load variation when the proposed PV systems are applied as DG1–DG3: (**a**) Frequency response; (**b**) output active power; (**c**) dc link voltage of the inverter; (**d**) exchanged power between the ES unit and dc link.

4.3. Case C: Short Circuit Fault—Conventional PV System

As Figure 10a depicts, the grid frequency, which is tracked by the conventional PV system, decreases until the fault is cleared and reaches the nadir of 49.82 Hz at 3 s. However, after the clearance of the fault, frequencies of the grid, DG1, DG2, and DG3 hardly change until the PFC is activated at 5 s. This shows that the conventional PV system fails to participate in frequency regulation. As Figure 10b depicts, the power imbalance resulting from the fault is counteracted only by the grid, while the conventional PV system is incapable of responding to the power imbalance, and outputs power without change after the fault occurs. The dc link voltage, illustrated in Figure 10c, is regulated during the fault to draw maximum power from the PV array.

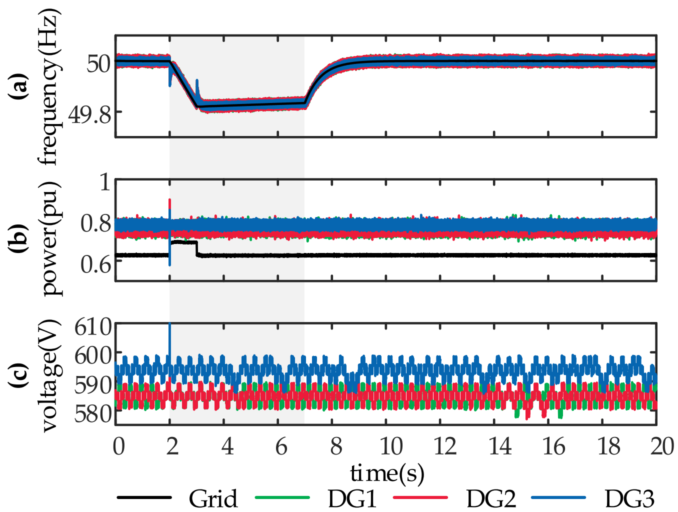

Figure 10. Responses to a short circuit fault when conventional PV systems are applied as DG1–DG3: (**a**) Frequency response; (**b**) output active power; (**c**) dc link voltage of the inverter.

4.4. Case D: Short Circuit Fault—Proposed PV System

System responses to a three-phase short circuit fault, where three proposed PV systems are integrated as DG1−DG3, are studied in this case, and given in Figure 11.

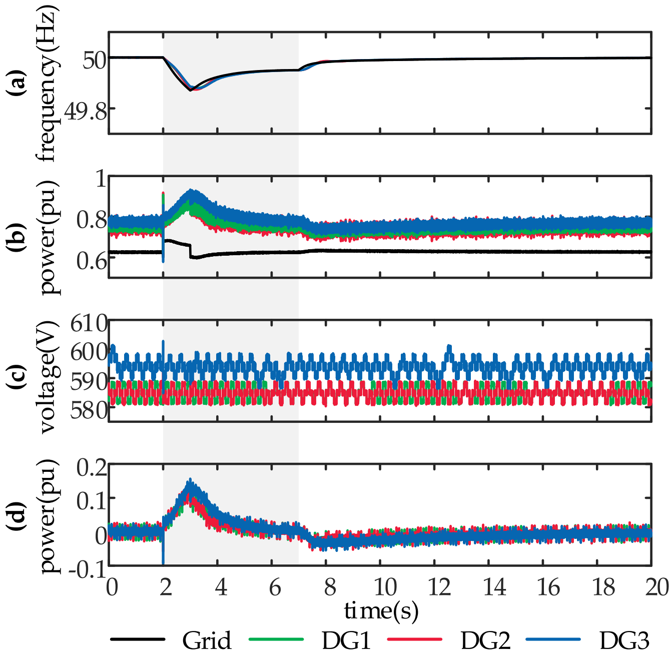

Figure 11. Responses to a short circuit fault when the proposed PV systems are applied as DG1–DG3: (**a**) Frequency response; (**b**) output active power; (**c**) dc link voltage of the inverter; (**d**) exchanged power between the ES unit and dc link.

The grid frequency, as shown in Figure 11a, decreases from the normal value of 50 Hz to the nadir of 49.87 Hz lasting from 2 s to 3 s. In comparison with Case C, a smaller ROCOF and slighter frequency deviation are caused by the fault in this case. It is perceived in Figure 11a that the grid frequency is regulated by the proposed PV system in the absence of PFC action during 3–7 s. As depicted in Figure 11b, the proposed PV system increases its output active power and moderates the power imbalance, while the conventional PV system fails to implement this function, as shown in Figure 10b.

Figure 11c illustrates the dc link voltage of the proposed PV system, which indicates that the proposed PV system is able to provide a stiff dc link voltage to emulate the inertia and perform MPPT. As depicted in Figure 11d, the incremental of P_{ES} is consistent with that of P_e shown in Figure 11b, verifying that the ES unit balances the power between the PV array and the inverter, which emulates the behavior of a rotor releasing kinetic energy when it's frequency declines.

4.5. Case E: Step of Solar Irradiance—Conventional PV System

As Figure 12a shows, the step of solar irradiance exerted on the PV array of DG 3 causes a sudden change of the power generated from the PV array in DG3. The dc link voltage of the inverter in DG 3 increases, as depicted in Figure 12b, to track U_{MPP} specified by the MPPT algorithm in the coordination control. Due to the lack of an energy buffer in the conventional PV system, DG3 injects the fluctuant PV power resulting from the solar irradiance step into the LV distribution network, and the output active power rises suddenly, as shown in Figure 12c. Figure 12d shows that the grid frequency deviates after the solar irradiance step until the PFC is activated.

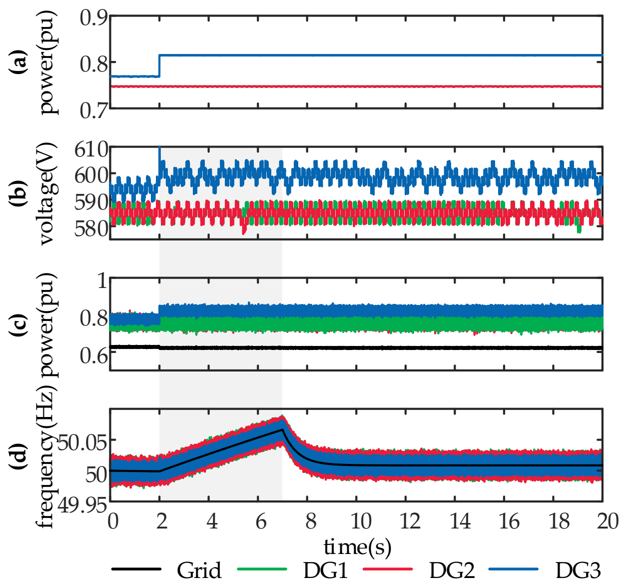

Figure 12. Responses to a step of solar irradiance when conventional PV systems are applied as DG1~DG3: (**a**) Power generated from the PV array; (**b**) dc link voltage of the inverter; (**c**) output active power; (**d**) frequency response.

4.6. Case F: Step of Solar Irradiance—Proposed PV System

Responses to the step of solar irradiance exerted on DG3 are studied in Figure 13 when three proposed PV systems are applied as DG1−DG3. After the solar irradiance steps, the power generated from the PV array in DG3 rises suddenly, as shown in Figure 13a, and the dc link voltage of DG3 increases to perform MPPT, as shown in Figure 13b. In comparison with *Case E*, the active power that DG3 feeds to the LV distribution network is filtered and rises smoothly, as depicted in Figure 13c, and the grid frequency deviates with a smaller ROCOF and lower zenith, as depicted in Figure 13d. Figure 13e shows that the exchanged power P_{ES} between the ES unit and the dc link decreases suddenly, and the ES unit of DG3 absorbs the surplus of PV production after the solar irradiance steps. P_{ES} eventually returns to zero, tracking the reference P_{ES_ref} to constrain the SOC, and the output active power P_e is finally equal to the power generated by the PV array P_{pv}.

It is demonstrated that the proposed PV system is able to smooth the power fed to the LV distribution network, even if the power generated by the PV array fluctuates suddenly.

Combining with the results in Cases A–F, Table 4 shows the following advantageous features of the proposed grid-supporting PV system as compared with the conventional PV system:

(1) The grid-supporting PV system, presenting as SGs from the point-of-view of the grid by mimicking SG characteristics with VSG control, can support the grid through mitigating the power imbalance between generation and consumption, and slowing down frequency dynamics with virtual inertia.
(2) Through emulating the droop characteristics of PFC and PVC, the grid-supporting PV system can participate in frequency regulation and voltage regulation.
(3) The proposed PV system has the functions of filtering the PV power and smoothing the power fed to the grid, which leads to a reduced impact of PV fluctuation on the grid.
(4) The grid-supporting PV system synchronizes with the grid through mimicking the synchronization mechanism of SGs, and thus the PLL, in which the delay may cause instability [34], is discarded in the proposed PV system.

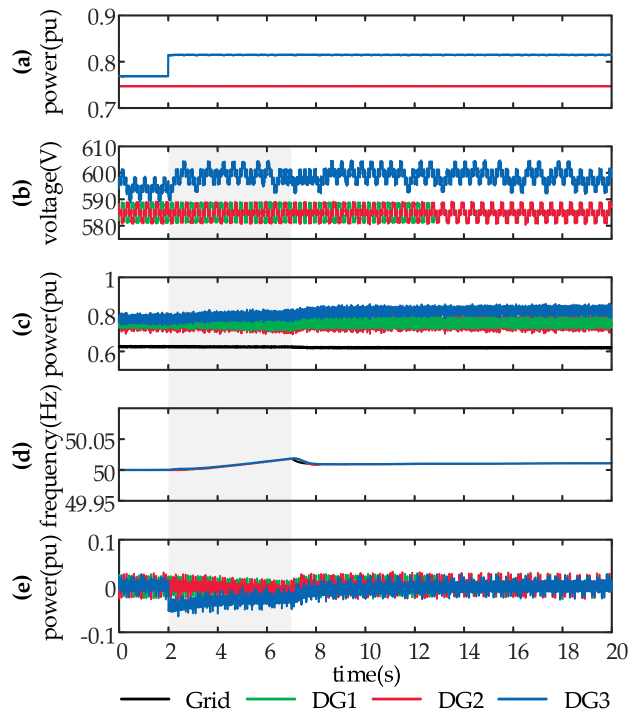

Figure 13. Responses to a step of solar irradiance when the proposed PV systems are applied as DG1–DG3: (**a**) Power generated from the PV array; (**b**) dc link voltage of the inverter; (**c**) output active power; (**d**) frequency response; (**e**) exchanged power between the ES unit and dc link.

Table 4. Advantages of the proposed grid-supporting PV system as compared with the conventional PV system.

Features	Conventional PV System	Proposed PV System
Emulating the characteristics of SGs to support the grid	×	√
Primary frequency control and primary voltage control	×	√
Smoothing the fluctuation of the power fed to the grid	×	√
PLL-less operation after initial synchronization	×	√

×: operating without the feature; √: operating with the feature.

5. Conclusions

A novel grid-supporting PV system, which operates as an inertia voltage source by emulating the characteristics of SGs, is proposed in this paper.

To present the PV system as a SG from the point-of-view of the grid, both the topology and the control scheme were investigated. An ES unit equipped with a bidirectional DC-DC converter was installed, which can mimic the function of a rotating rotor for kinetic energy and buffer the imbalance of the PV power. On the other hand, the coordination control, DC-DC control, and VSG control were employed in the proposed system. The coordination control is able to constrain the SOC of the ES unit and calculate the voltage at the maximum power point of the PV array. The DC-DC control can perform the regulation of the dc link voltage to realize MPPT, and the VSG control is capable of equipping the interface inverter with SG characteristics.

To guide the tuning of the parameters, the system performance was analyzed with the variation parameter values. It was found that the inertia constant H plays an important role in determining the settling time, and that the system damping mainly depends on $D + K_{\omega}$. Furthermore, the stability constraint was formulated as Equation (31), which should be satisfied to guarantee the stability of the system.

Results of case studies conducted on the modified CIGRE LV network benchmark verify the grid-supporting PV system. Compared with the conventional PV system, the grid-supporting PV system is advantageous in the following areas:

(1) The VSG control and the ES unit capacitate the interface inverter of the proposed inverter to mimic SG characteristics, slowing down frequency response with inertia, and moderating the power imbalance between generation and consumption.
(2) The emulation of the droop characteristics of PFC and PVC capacitates the grid-supporting PV system to contribute to frequency regulation and voltage regulation of EPS.
(3) In the conventional PV system, the power fed to the grid must be equal to the power generated from the PV array. However, the installation of the ES unit in the grid-supporting PV system spares this embarrassment. Through the installed ES unit and the control scheme, the function of filtering the PV power and smoothing the PV system output power, which reduces the impact of PV fluctuations on the grid, is implemented in the proposed grid-supporting PV system.
(4) With the VSG control, the interface inverter of the grid-supporting PV system mimics not only the inertia and frequency damping of SGs, but also the synchronization mechanism of SGs. Beneficially, the impact of the PLL on the stability is eliminated, which leads to the proposed PV system being more compatible with EPS than the conventional PV system that employs the PLL.

The topology, the control scheme, and the stability constraint for parameters are presented in this paper. In future, the method for optimizing the capacity of the ES unit under different conditions, where the values of H, D, and K_{ω}, and the capacity of the PV array vary, need to be obtained in order to reduce costs. As the analysis indicates, the grid impedance has impacts on the stability of the system with the Q-E droop control. How to reduce or avoid these impacts is also set as one of our future research directions.

Author Contributions: H.X. and J.S. provided the original idea for this paper. H.X., N.L., and Y.S. organized the manuscript and attended the discussions when analysis and verification were carried out. All the authors gave comments and suggestions on the writing and descriptions of the manuscript.

Funding: This research was supported partly by the National Key Research and Development Program of China (2017YFB0903503), the National Science Foundation of China (51677050) and Double First Class Project for Independent Innovation and Social Service Capabilities (45000-411104/012).

Conflicts of Interest: The authors declare no conflict of interest.

Abbreviations

The following abbreviations are used in this manuscript:

EMF	Electromotive force
EPS	Electric power systems
ES	Energy storage
MPPT	Maximum power point tracking
PFC	Primary frequency control
PLL	Phase-locked loops
PV	Photovoltaic
PVC	Primary voltage control
RES	Renewable energy sources
ROCOF	Rate of change of frequency
SG	Synchronous generator
SOC	State of charge
VSG	Virtual synchronous generator

References

1. Pintér, G.; Baranyai, N.H.; Wiliams, A.; Zsiborács, H. Study of Photovoltaics and LED Energy Efficiency: Case Study in Hungary. *Energies* **2018**, *11*, 790. [CrossRef]
2. Egwebe, A.M.; Fazeli, M.; Igic, P.; Holland, P.M. Implementation and stability study of dynamic droop in islanded microgrids. *IEEE Trans. Energy Convers.* **2016**, *31*, 821–832. [CrossRef]
3. Zsiborács, H.; Baranyai, N.H.; András, V.; Háber, I.; Pintér, G. Economic and Technical Aspects of Flexible Storage Photovoltaic Systems in Europe. *Energies* **2018**, *11*, 1445. [CrossRef]
4. Radwan, A.A.A.; Mohamed, Y.A.R.I. Power synchronization control for grid-connected current-source inverter-based photovoltaic systems. *IEEE Trans. Energy Convers.* **2016**, *31*, 1023–1036. [CrossRef]
5. Nižetić, S.; Papadopoulos, A.M.; Tina, G.M.; Rosa-Clot, M. Hybrid energy scenarios for residential applications based on the heat pump split air-conditioning units for operation in the Mediterranean climate conditions. *Energy Build.* **2017**, *140*, 110–120. [CrossRef]
6. Rocabert, J.; Luna, A.; Blaabjerg, F.; Rodríguez, P. Control of power converters in AC microgrids. *IEEE Trans. Power Electron.* **2012**, *27*, 4734–4749. [CrossRef]
7. Delille, G.; Francois, B.; Malarange, G. Dynamic frequency control support by energy storage to reduce the impact of wind and solar generation on isolated power system's inertia. *IEEE Trans. Sustain. Energy* **2012**, *3*, 931–939. [CrossRef]
8. Kroposki, B.; Johnson, B.; Zhang, Y.; Gevorgian, V.; Denholm, P.; Hodge, B.; Hannegan, B. Achieving a 100% renewable grid: Operating electric power systems with extremely high levels of variable renewable energy. *IEEE Power Energy Mag.* **2017**, *15*, 61–73. [CrossRef]
9. Wesenbeeck, M.P.N.; de Haan, S.W.H.; Varela, P.; Visscher, K. Grid tied converter with virtual kinetic storage. In Proceedings of the IEEE Bucharest PowerTech, Bucharest, Romania, 28 June–2 July 2009.
10. Eftekharnejad, S.; Vittal, V.; Heydt, G.T.; Keel, B.; Loehr, J. Impact of increased penetration of photovoltaic generation on power systems. *IEEE Trans. Power Syst.* **2013**, *28*, 893–901. [CrossRef]
11. Ulbig, A.; Borsche, T.S.; Andersson, G. Impact of low rotational inertia on power system stability and operation. In Proceedings of the IFAC World Congress, Capetown, South Africa, 24–29 August 2014.
12. Beck, H.P.; Hesse, R. Virtual synchronous machine. In Proceedings of the 9th International Conference on Electrical Power Quality Utilizations, Barcelona, Spain, 9–11 October 2007.
13. VSG Control Algorithms: Present Ideas. Available online: http://www.vsync.eu.ProjectVSYNC (accessed on 22 March 2016).
14. Zhong, Q.C.; Weiss, G. Synchronverters: Inverters that mimic synchronous generators. *IEEE Trans. Ind. Electron.* **2011**, *58*, 1259–1267. [CrossRef]
15. Sakimoto, K.; Miura, Y.; Ise, T. Stabilization of a power system with a distributed generator by a virtual synchronous generator function. In Proceedings of the IEEE 8th International Conference Power Electronics ECCE Asia (ICPE & ECCE), Jeju, Korea, 30 May–3 June 2011.
16. Bevrani, H.; Ise, T.; Miura, Y. Virtual synchronous generators: A survey and new perspectives. *Int. J. Electr. Power Energy Syst.* **2014**, *54*, 244–254. [CrossRef]
17. Natarajan, V.; Weiss, G. Synchronverters with better stability due to virtual inductors, virtual capacitors and anti-windup. *IEEE Trans. Ind. Electron.* **2017**, *64*, 5994–6004. [CrossRef]
18. Alipoor, J.; Miura, Y.; Ise, T. Power system stabilization using virtual synchronous generator with alternating moment of inertia. *IEEE J. Emerg. Sel. Top. Power Electron.* **2015**, *3*, 451–458. [CrossRef]
19. Li, D.; Zhu, Q.; Lin, S.; Bian, X.Y. A self-adaptive inertia and damping combination control of VSG to support frequency stability. *IEEE Trans. Energy Convers.* **2017**, *32*, 397–398. [CrossRef]
20. Alipoor, J.; Miura, Y.; Ise, T. Stability Assessment and Optimization Methods for Microgrid with Multiple VSG Units. *IEEE Trans. Smart Grid* **2016**, *9*, 1462–1471. [CrossRef]
21. Torres, L.M.A.; Lopes, L.A.C.; Morán, T.L.A.; Espinoza, C.J.R. Self-tuning virtual synchronous machine: A control strategy for energy storage systems to support dynamic frequency control. *IEEE Trans. Energy Convers.* **2014**, *29*, 833–840. [CrossRef]
22. Dong, S.; Chen, Y.C. Adjusting synchronverter dynamic response speed via damping correction loop. *IEEE Trans. Energy Convers.* **2017**, *32*, 608–619. [CrossRef]
23. Suul, J.A.; D'Arco, S.; Guidi, G. Virtual synchronous machine-based control of a single-phase bi-directional battery charger for providing vehicle-to-grid services. *IEEE Trans. Ind. Appl.* **2016**, *52*, 3234–3244. [CrossRef]

24. Fang, J.; Tang, Y.; Li, H.; Li, X. A battery/ultracapacitor hybrid energy storage system for implementing the power management of virtual synchronous generators. *IEEE Trans. Power Electron.* **2018**, *33*, 2820–2824. [CrossRef]
25. Liu, J.; Miura, Y.; Bevrani, H.; Ise, T. Enhanced virtual synchronous generator control for parallel inverters in microgrids. *IEEE Trans. Smart Grid* **2017**, *8*, 2268–2277. [CrossRef]
26. Alam, M.J.E.; Muttaqi, K.M.; Sutanto, D. A novel approach for ramp-rate control of solar PV using energy storage to mitigate output fluctuations caused by cloud passing. *IEEE Trans. Energy Convers.* **2014**, *29*, 507–518. [CrossRef]
27. Thang, T.V.; Ahmed, A.; Kim, C.I.; Park, J.H. Flexible system architecture of stand-alone PV power generation with energy storage device. *IEEE Trans. Energy Convers.* **2015**, *30*, 1386–1396. [CrossRef]
28. Fuente, D.V.; Trujillo Rodríguez, C.L.; Garcerá Figueres, G.E.; Gonzalez, R.O. Photovoltaic power system with battery backup with grid-connection and islanded operation capabilities. *IEEE Trans. Ind. Electron.* **2013**, *60*, 1571–1581. [CrossRef]
29. Kadri, R.; Gaubert, J.; Champenois, G. An improved maximum power point tracking for photovoltaic grid-connected inverter based on voltage-oriented control. *IEEE Trans. Ind. Electron.* **2011**, *58*, 66–75. [CrossRef]
30. Esram, T.; Chapman, P.L. Comparison of photovoltaic array maximum power point tracking techniques. *IEEE Trans. Energy Convers.* **2007**, *22*, 439–449. [CrossRef]
31. Yazdani, A.; Fazio, A.R.D.; Ghoddami, H.; Russo, M.; Kazerani, M.; Jatskevich, J.; Strunz, K.; Leva, S.; Martinez, J.A. Modeling guidelines and a benchmark for power system simulation studies of three phase single-stage photovoltaic systems. *IEEE Trans. Power Deliv.* **2011**, *26*, 1247–1264. [CrossRef]
32. Kundur, P.; Balu, N.J.; Lauby, M.G. *Power System Stability and Control*; McGraw-Hill Inc.: New York, NY, USA, 1994; ISBN 9780070359581.
33. Strunz, K.; Abbasi, E.; Fletcher, R.; Hatziargyriou, N.D. *Benchmark Systems for Network Integration of Renewable and Distributed Energy Resources*; CIGRÉ TF C6.04.02, Technical Report 575; CIGRE: Paris, France, 2014.
34. Norouzi, A.H.; Sharaf, A.M. Two control scheme to enhance the dynamic performance of the STATCOM and SSSC. *IEEE Trans. Power Deliv.* **2005**, *20*, 435–442. [CrossRef]